2025 World Journal of Innovation and Modern Technology, Vol. 8, Issue 6 (Jun)
ISSN 2682-5910
DOI: 10.53469/wjimt.2025.08(06).13

An Evaluation of Carbon Emissions Based on the Hidden Markov Model

Fucheng Tan[1], Jinhong Chen[1], Juyao Yin[1], Shengkui Xi[1], Yutao Xie[2], Yan Li[1,*]

[1]School of Science, North China University of Science and Technology, Tangshan 063000, Hebei, China
[2]School of Computer Science, North China University of Science and Technology, Tangshan 063000, Hebei, China
Correspondence Author

Abstract: ***To address the challenge of assessing carbon emissions in the iron ore sintering process, characterized by dynamic complexity, strong temporal correlations, and multi-stage coupling, this study innovatively introduces the Hidden Markov Model (HMM) into the field of carbon emission analysis. We propose a method for process stage identification and carbon emission modeling based on a Gaussian Hidden Markov Model (Gaussian HMM). The model defines the four stages of the sintering process as hidden states and uses six-dimensional flue gas monitoring data (temperature, SO_2 concentration, NO concentration, NOx concentration, O_2 content, CO concentration) as the observation sequence, with Gaussian distributions describing the emission characteristics of each stage. The research employs the Random Forest algorithm to impute missing values and correct outliers in the raw data, followed by standardization to eliminate scale differences. Model parameters are initialized using Maximum Likelihood Estimation (MLE) and iteratively optimized via the Forward-Backward and Baum-Welch algorithms to enhance the model's fitting capability for complex temporal data. The Viterbi algorithm dynamically decodes the hidden state sequence, enabling an online "predict-until-cooling" monitoring strategy. This strategy accurately determines the optimal cooling timing to balance combustion efficiency with the reaction endpoint. This approach prevents incomplete iron ore combustion and low raw material utilization, while simultaneously reducing emissions of harmful gases and greenhouse gases, thereby achieving the goal of lowering carbon emissions. It provides technical support for the refined management of carbon emissions.***

Keywords: Hidden Markov Model; Carbon Emissions; Forward–Backward Algorithm; Baum–Welch Algorithm; Viterbi Algorithm.

1. INTRODUCTION

On September 22, 2020, General Secretary Xi Jinping delivered a speech during the General Debate of the 75th Session of the United Nations General Assembly, in which he clearly stated China's strategic goal of "enhancing its nationally determined contributions, adopting more forceful policies and measures, striving to peak carbon dioxide emissions before 2030, and making all-out efforts to achieve carbon neutrality before 2060." According to data released by the World Steel Association, in 2023 global crude steel production reached 1.8882 billion tonnes, of which China's output was 1.0191 billion tonnes—accounting for over 50 percent of the world total [1]. From an industry-structure perspective, the steel sector ranks first in carbon emissions among the 31 detailed subdivisions of manufacturing, contributing approximately 15 percent of China's total emissions. As a key emissions-intensive sector, the green and low-carbon transformation of the steel industry has become imperative. Within steelmaking processes, sintering represents the second-largest energy-consuming operation and bears a significant share of total carbon emissions; therefore, controlling emissions from the sintering process is directly linked to steel enterprises' progress toward their reduction targets.

Iron-ore sintering is the principal source of gaseous pollutant emissions in the steel-making process. Its emissions of particulate matter, SO_2, NO_x, and CO account for approximately 20 percent, 70 percent, 48 percent, and 36.06 percent, respectively, of total gaseous emissions in the steel industry [2]. In April 2019, the Ministry of Ecology and Environment, together with other ministries, issued the "Opinions on Promoting Ultra-Low Emissions in the Steel Industry" (Huan Daqi [2019] No. 35), which stipulate that emissions of particulate matter, SO_2, NO_x, and dioxins in the sinter machine hood flue gas must not exceed 10 mg/m³, 35 mg/m³, 50 mg/m³, and 0.5 ng/m³, respectively [3]. Although, in key regions, steel enterprises have now attained these ultra-low emission standards for particulate matter, SO_2, and NO_x—with pollutant emission intensities decreasing year by year—the inherent characteristics of sinter flue gas and the process itself result in an initial CO concentration (calculated on an 8 000 mg/m³ basis) that is roughly 800 times, 228 times, and 160 times higher than the ultra-low emission limits for particulate matter, SO_2, and NO_x, respectively [4], leading to massive CO releases. Related studies confirm that carbon monoxide, as a highly toxic gas, poses multiple health hazards. Its toxic effects not only directly impair cardiovascular and respiratory function but, under sunlight, CO also engages in complex photochemical reactions with non-methane hydrocarbons (NMHC) and nitrogen oxides (NO_x) in the atmosphere to produce photochemical

smog dominated by ozone. This secondary pollutant not only causes crop yield reductions and accelerated corrosion of building materials but also induces acute eye and respiratory irritation in humans, which in severe cases can be life-threatening.

2. SINTERING PROCESS FLOW

Iron-ore sintering is a thermal agglomeration process in which iron ore fines, recovered iron-making by-products, fluxing agents, slag conditioners and solid fuel (coke) are blended, ignited on a sintering strand and ultimately fused into clinker-sized agglomerates [5]. The feedstock typically comprises beneficiated concentrate from low-grade ores, crushed fines of high-grade ores and iron-bearing recycled materials (e.g. blast-furnace and converter dust, rolling-mill scale), combined with fluxes such as limestone and dolomite, and fuels like coke breeze or anthracite. After precise proportioning, mixing and granulation to form a homogeneous charge, the material is evenly distributed onto the strand by a feed system. Ignition followed by negative-pressure suction then initiates high-temperature solidification.

During sintering, multiple coupled multiphase reactions occur. As preheated air penetrates the hot bed, the combustion zone reaches 1250–1500°C, driving intense oxidation of the solid fuel and releasing the thermal energy required for agglomeration. The descending flue gas then passes sequentially through the drying layer (200–400 °C), evaporating free moisture, and the preheating layer (400–800°C), decomposing carbonates and reducing iron oxides. Concurrently, CaO, SiO_2 and other oxides undergo solid–liquid reactions in the combustion zone to form complex mineral phases, while impurities such as sulfur and arsenic are oxidized and captured in the molten flux. Finally, the liquid phase cools under a temperature gradient, creating an interwoven mineral structure and yielding high-strength sinter.

In contemporary production, belt-type suction sinter machines dominate. Modern belt-type sintering integrates raw-material pretreatment (optimizing fuel granularity), enhanced granulation and hot-flue-gas recycling. These advancements reduce solid-fuel consumption and achieve coordinated control of pollutants, propelling sinter production toward a low-carbon, high-efficiency paradigm.

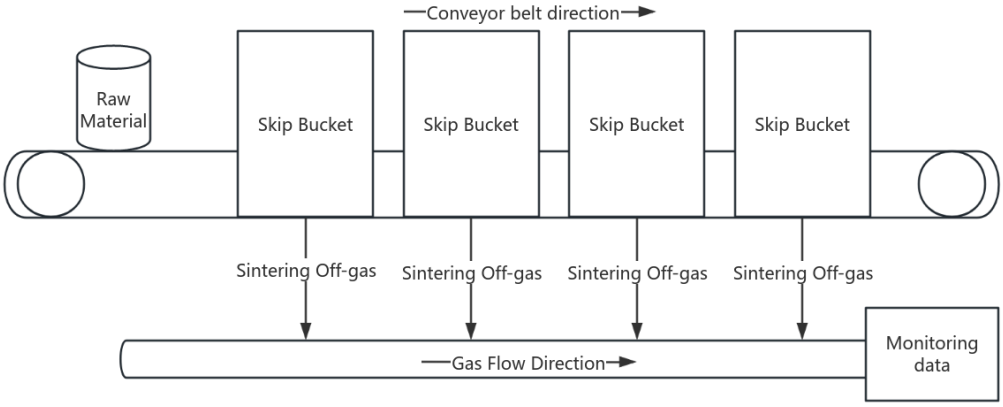

Figure 1: Simulation of belt exhaust sintering machine

In the belt-type suction sintering process, operation proceeds from top to bottom through the depth of the sinter bed, which is conventionally subdivided into five strata—beginning with the sinter layer at the top, followed by the combustion zone, the drying-and-preheating zone, the over-wet layer and, finally, the raw-material layer at the bottom. As sintering advances, the latter four zones successively disappear, leaving only the consolidated sinter layer as the finished product. Within this bed, coke particles are dispersed irregularly and burn in a manner intermediate between that of isolated pellets and a cohesive coke bed, characterizing a heterogeneous reaction system. Throughout the sintering cycle, five distinct reaction pathways overlap and interact [6]:

$$(2C + O_2 = 2CO_2 \quad \Delta G^{\Theta} = -395350 - 0.54T \tag{1}$$

$$(2C + O_2 = 2CO \quad \Delta G^{\Theta} = -228800 - 171.54T \tag{2}$$

$$(2CO + O_2 = 2CO_2 \quad \Delta G^{\Theta} = -561900 + 170.46T \tag{3}$$

$$(CO_2 + C = 2CO \quad \Delta G^{\Theta} = 166550 - 171.00T \tag{4}$$

$$(C + H_2O = CO + H_2 \quad \Delta G^{\Theta} = 31378 - 31.971T \tag{5}$$

Because each reaction has a different Gibbs free energy at varying temperatures, the duration and intensity of these reactions likewise differ significantly. Under the driving force of negative-pressure suction, oxygen-laden gas streams penetrate the sinter bed from top to bottom, following gas–solid two-phase convective mass-transfer laws. When oxygen reacts with coke at the particle surface, a gaseous boundary layer forms at the reaction interface, severely limiting both the efficiency of O_2 transport to the surface and the back-diffusion of reaction products (CO/CO_2). Consequently, the kinetics of carbon combustion are governed not only by the combustion temperature but also by the diffusion rate of O_2 toward the reaction front and the reverse diffusion efficiency of CO_2—parameters that are intrinsically coupled to the bed's permeability characteristics and the applied gas-flow velocity.

Moreover, variations in raw-material composition exert a pronounced influence on these reaction pathways. When the sulfur content of the feed is elevated, accelerated decomposition of sulfides in the high-temperature zone causes a sharp rise in SO_2 formation; this necessitates optimizing thermal-engineering parameters to shorten residence time in the hottest region and thereby suppress sulfur oxidation. Conversely, carbon-rich fuels require an expanded combustion zone width to ensure complete coke oxidation, minimizing the risk of residual CO from incomplete combustion. It is important to note that, although intensified suction can improve sintering efficiency, excessively high gas-flow rates reduce the oxidation time available to fuel particles—allowing unburnt CO to entrain rapidly into the off-gas stream and, in effect, exacerbate CO fugitive emissions.

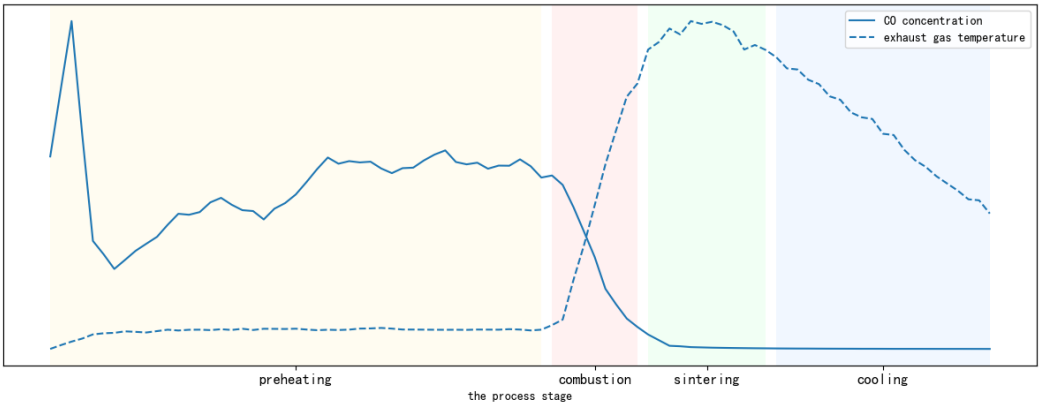

Figure 2: CO concentration and exhaust gas temperature vary with process stage

By correlating CO concentration with flue-gas temperature, the sintering process can be divided into four stages: preheating, combustion, sintering, and cooling. During preheating, the over-wet layer keeps temperatures relatively low. As ignition initiates, the combustion zone and drying-preheating zone gradually develop and thicken, intensifying carbon combustion and generating increasing volumes of CO. Consequently, the CO mass concentration rises sharply to a pronounced peak. Once ignition ends, a surge of air drawn in by negative-pressure suction strengthens the oxidizing atmosphere, driving more complete carbon combustion and causing the CO concentration to plunge. As suction sintering continues, an increasing fraction of the bed softens and melts, thickening the over-wet layer, which in turn impairs bed permeability and weakens oxidation. Incomplete combustion then causes CO levels to climb rapidly into a high-concentration regime. When the process reaches the full combustion phase, the over-wet layer vanishes and temperature spikes: the sinter layer proportion grows while the combustion and drying-preheating zones shrink, restoring bed permeability and oxidizing conditions so that carbon burns out fully and CO concentration falls precipitously. After the transition into the sintering phase, the combustion zone disappears altogether and CO concentrations remain low. Finally, during cooling, temperatures decline and CO concentrations approach zero.

In sintering, "under-burning" refers to insufficient combustion that leaves raw materials incompletely reacted and iron minerals inadequately consolidated, resulting in low sinter strength, high pulverulence, and reduced material utilization. Conversely, "over-burning" arises when high temperatures persist too long or cooling lags, causing excessive mineral melting and lattice distortion; this not only increases energy consumption but also exacerbates emissions of CO, SO_2, and greenhouse gases. Accurately determining the optimal cooling point—thereby dynamically balancing combustion efficiency against reaction completion—prevents both under-burning and over-burning, reduces harmful and greenhouse gas emissions, and ultimately lowers carbon output.

3. HIDDEN MARKOV MODEL

The Hidden Markov Model (HMM) is a probabilistic modeling method based on a double stochastic process, first proposed by Baum, Welch and others in the mid-1970s. It constructs a temporal-data analysis framework by dynamically linking hidden state transitions with observable outputs, and it has since been widely applied in fields such as speech-signal processing, biomedical-data analysis, and industrial-system fault monitoring [7–8]. The core architecture of the HMM consists of two coupled stochastic processes: one is the hidden-state sequence, which evolves over time according to the Markov property (memoryless transitions); the other is the observation sequence, which maps each hidden state to measurable outputs via probability-density functions. In HMM modeling, the observer has access only to the explicit observation data driven by the hidden-state sequence, while the true sequence of state transitions must be inferred through probabilistic inversion algorithms (e.g. Viterbi decoding). This reverse inference of the hidden-state chain from the observation sequence constitutes the essence of the Hidden Markov process. To fully specify an HMM, the following symbols or variables must be defined:

An HMM is represented by the triplet $\lambda = (\Pi, A, B)$:

$S = \{1,2,\ldots,K\}$, where S denotes the set of hidden states and K is the total number of states.

$\Pi = \{\pi_i\}, 1 \le i,j \le K$, where π_i is the probability that the initial state at time t = 1 is i.

$A = \{a_{ij}\}, 1 \le i,j \le K$, where a_{ij} is the probability of transitioning from state i to state j.

$B = \{b_{ij}\}, 1 \le i,j \le K$, where b_{ij} is the probability of emitting observation j when in hidden state i.

Given an HMM $\lambda = (\Pi, A, B)$, n observation sequence $O = \{o_1, o_2, \ldots, o_T\}$ and a corresponding state sequence $S = \{s_1, s_2, \ldots, s_T\}$, The probability of generating the observation sequence is given by:

$$P(O, S|\lambda) = \pi_{S1} \bullet \left(\prod_{t=1}^{T-1} a_{s_t s_{t+1}}\right) \bullet \left(\prod_{t=1}^{T} b_{s_t}(o_t)\right)$$

This formula describes the probability of, under a given HMM, first generating a state sequence and then producing the observation sequence from those states. The HMM infers the most likely hidden-state path and its probability from the observation sequence, as illustrated in the figure below:

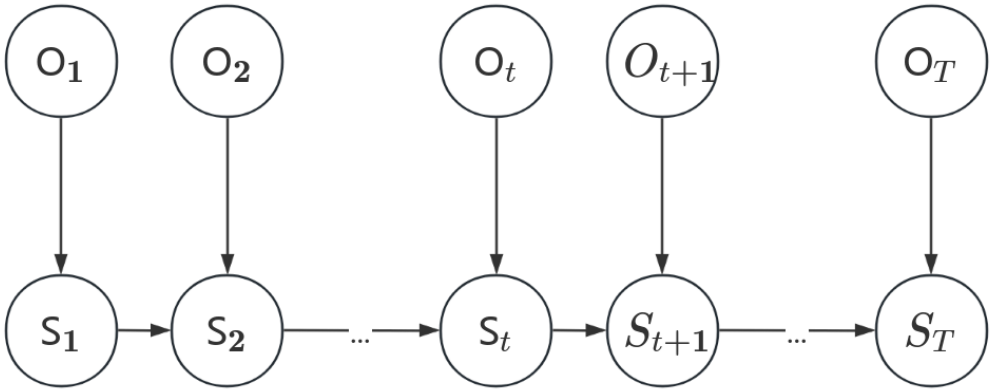

Figure 3: Conceptual diagram of the Hidden Markov model

In the iron-ore sintering process, the six-dimensional observation signals—flue-gas temperature, SO_2, NO, NO_x, O_2, and CO—exhibit multimodal distributions, temporal correlations, and noise interference as the process progresses through its four stages (preheating → combustion → sintering → cooling). To accurately identify the latent operating conditions in each stage, characterize the dynamics of emissions, and provide decision support for carbon-emission control, it is necessary to employ a temporal model capable both of capturing hidden-stage transitions and of handling continuous, multidimensional observations. The Gaussian Hidden Markov Model (Gaussian HMM) is an extension of the classical HMM in which the observation-likelihood functions are Gaussian (either unimodal or multimodal). In a Gaussian HMM, observations $b_j(o_t)$ are no longer treated as discrete values but are modeled by Gaussian distributions—each hidden state s_j being associated with its own Gaussian emission distribution:

$$b_j(o_t) = N(o_t|\mu_i, \sum_i) = \frac{1}{\sqrt{(2\pi)^k|\sum_j|}} exp\left(-\frac{1}{2}(o_t - \mu_j)^T \Sigma_j^{-1}(o_t - \mu_j)\right)$$

It can capture the average emission characteristics of each stage via the mean μ_i, and characterize the dynamic interdependence and uncertainty among the indicators via the covariance Σ_i. The parameter set for the Gaussian HMM emission distributions is:

$$B = \{(\mu_i, \sum_i)|i = 1, \ldots, n\}$$

Therefore, in a Gaussian HMM, the probability of generating the observation sequence$O = \{o_1, o_2, \ldots, o_T\}$ is given by:

$$P(O, \lambda) = \sum_S [\pi_{S_1} \bullet (\prod_{t=1}^{T-1} a_{s_t s_{t+1}}) \bullet (\prod_{t=1}^{T} N(O_t|\mu_{S_t}, \Sigma_{S_t}))]$$

4. ALGORITHM WORKFLOW

In this study, a Python program was developed to read minute-level flue-gas monitoring data from the sintering process—including temperature, SO_2, NO, NO_x, O_2, and CO—and to sort these observations in chronological order. Maximum likelihood estimation (MLE) was then used to initialize the parameters of a Gaussian HMM. Next, the Baum–Welch algorithm iteratively re-estimated the model parameters until the increase in log-likelihood fell below a preset threshold or a maximum number of iterations was reached. The trained model was then applied to new observation sequences: the Viterbi algorithm decoded the most likely hidden-state sequence and predicted each minute's state from a specified start time until the first detection of the "cooling" stage. Finally, predictions were compared against true labels to generate a classification report and confusion matrix, thereby evaluating the model's classification performance across the four stages (preheating, combustion, sintering, cooling) and its accuracy in identifying the onset of cooling.

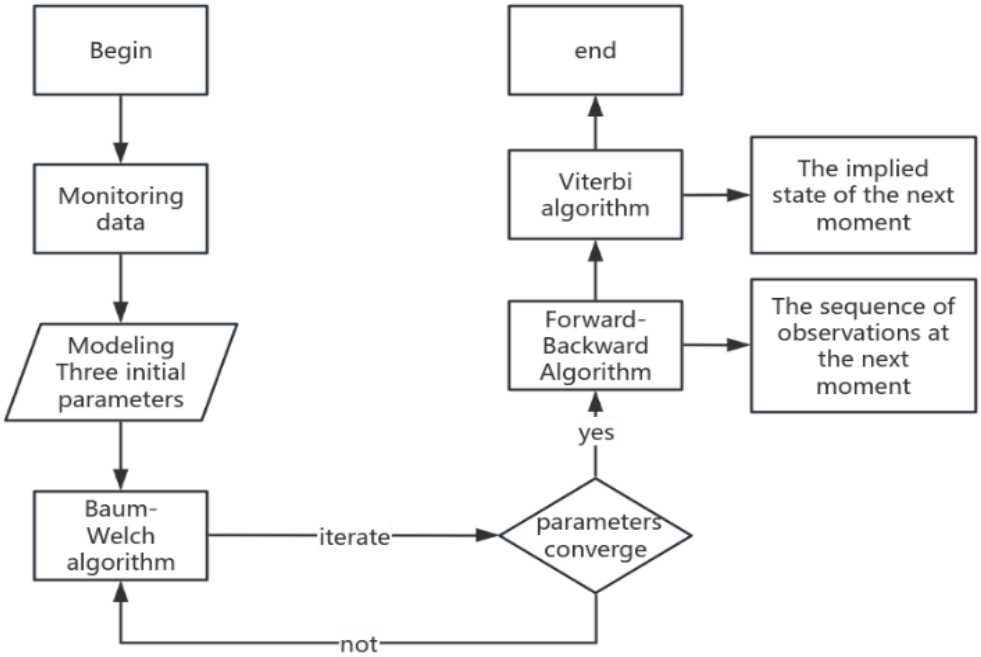

Figure 4: Algorithm flowchart

Step1: Analyze and organize the flue-gas monitoring dataset of the sintering process to construct the initial dataset.

Step2: Apply a random forest algorithm to the initial dataset to impute and correct missing and anomalous data, thereby improving the efficiency and accuracy of the HMM model.

Step3: By analyzing the correspondence between the sintering process's carbon-emission assessment and the Hidden Markov Model, treat the key stages of the sintering process (preheating, combustion, sintering, cooling) as hidden states in the latent layer, and use the filtered monitoring data as observable states in the observation layer. Then initialize the HMM's parameters $\lambda = (\Pi, A, B)$ using maximum likelihood estimation (MLE).

Step4: The Baum–Welch algorithm [9] is employed to iteratively estimate the mean vectors and covariance matrices of the Gaussian emission distributions for each hidden state by maximizing the likelihood of the observed data until the model parameters converge, thereby yielding the optimal Hidden Markov Model.

Step5: Using the trained model and the currently available observation sequence, the next most likely observation is predicted via probabilistic computation, with the outcome of highest probability selected as the prediction output. Finally, using the optimal model parameters thus obtained and a new observation sequence V, the Viterbi algorithm [10] is applied to derive the optimal hidden–state sequence S, from which the cooling onset is inferred.

5. EMPIRICAL STUDY

5.1 Dataset Preparation

5.1.1 Data Selection

The data originate from sinter-cup experiments conducted in the central laboratory of Hebei Yongyang Special Steel Group Co., Ltd. Three complete sintering runs were extracted from the flue-gas monitoring system's datasets. From these, six indicators—flue-gas temperature, SO_2 concentration, NO concentration, NO_x concentration, O_2 content, and CO concentration—were selected to form a new dataset.

5.1.2 Data Preprocessing

After imputing and correcting missing and anomalous values via a random-forest algorithm, all features were standardized to the same scale to prevent high-magnitude variables (e.g., CO concentration in mg/m³) from overwhelming low-magnitude ones (e.g., O_2 content in percent). For maximum-likelihood estimation under a Gaussian model, standardized features share similar distributions across dimensions, which prevents excessively large or small gradients, significantly accelerates algorithmic convergence, and improves numerical stability. Moreover, standardization brings feature variances to the same order of magnitude, making the covariance matrices more readily positive-definite and comparable.

5.1.3 Train–Test–Validation Split

Based on CO concentration and flue-gas temperature profiles, each of the three runs was labeled with one of four states—0, 1, 2, or 3—corresponding respectively to the preheating, combustion, sintering, and cooling stages. These labeled datasets were stored in three sheets: Sheet1, Sheet2, and Sheet3. Sheet1 was designated as the training set for fitting and optimizing the parameters of the Gaussian Hidden Markov Model. Sheet2 served as the test set to evaluate the model's ability to correctly identify the four process stages. Sheet3 functioned as the validation set to verify the model's accuracy in predicting hidden states and determining the optimal onset of the cooling stage.

5.2 Parameter Estimation

5.2.1 Initial Parameter Setting

Because the Baum–Welch algorithm is highly dependent on its starting values, maximum likelihood estimation (MLE) is used to initialize the HMM's parameters $\lambda = (\Pi, A, B)$,

$$\Pi = [1, 0, 0, 0]^T$$

$$A = \begin{bmatrix} 0.9787 & 0.0213 & 0 & 0 \\ 0 & 0.8888 & 0.1112 & 0 \\ 0 & 0 & 0.9167 & 0.0833 \\ 0 & 0 & 0 & 1 \end{bmatrix}$$

After normalization, the emission distributions Bestimated by MLE—that is, the mean vectors (μ_i) and covariance matrices (Σ_i) of the Gaussian emission distributions for each state—are as follows:

$$\mu_0 = \begin{pmatrix} -0.8353 \\ -0.2483 \\ 0.8026 \\ 0.8097 \\ -0.7966 \\ 0.8023 \end{pmatrix} \mu_1 = \begin{pmatrix} 0.2229 \\ 2.3957 \\ 0.0819 \\ 0.0263 \\ -0.1443 \\ -0.0346 \end{pmatrix} \mu_2 = \begin{pmatrix} 1.6583 \\ -0.1314 \\ -1.1205 \\ -1.1187 \\ 1.1067 \\ -1.1108 \end{pmatrix} \mu_3 = \begin{pmatrix} 0.8263 \\ -0.3958 \\ -1.1912 \\ -1.1842 \\ 1.2123 \\ -1.1460 \end{pmatrix}$$

$$\sum 0 = \begin{pmatrix} 0.001220 & 0 & 0 & 0 & 0 & 0 \\ 0 & 0.506051 & 0 & 0 & 0 & 0 \\ 0 & 0 & 0.231292 & 0 & 0 & 0 \\ 0 & 0 & 0 & 0.232077 & 0 & 0 \\ 0 & 0 & 0 & 0 & 0.222268 & 0 \\ 0 & 0 & 0 & 0 & 0 & 0.266865 \end{pmatrix}$$

Denoted as:

$$\Sigma_0 = \text{diag}(0.001220,0.506051,0.231292,0.232077,0.222268,0.266865)$$

Similarly,

$$\Sigma_1 = \text{diag}(0.540744,0.664762,0.317168,0.304536,0.294261,0.419682)$$

$$\Sigma_2 = \text{diag}(0.008511,0.096996,0.006034,0.005086,0.015841,0.002275)$$

$$\Sigma_3 = \text{diag}(0.161632,0.000816,0.00000049,0.00000389,0.006945,0.0000027)$$

5.2.2 Parameter Optimization

The Baum–Welch algorithm is an Expectation–Maximization (EM) method for estimating the parameters of an HMM. When the model parameters (initial-state distribution, state-transition matrix, and emission matrix) are unknown, the Baum–Welch algorithm can infer them from a given observation sequence. It proceeds by iteratively executing two steps:

E-step (Expectation): Using the current model parameters, compute the expected state-occupancy probabilities via the forward–backward algorithm.

M-step (Maximization): Maximize the expected log-likelihood to update the model parameters.

The detailed procedure is as follows:

1) Initialization:
Set initial estimates for $\lambda = (\Pi, A, B)$.

2) Expectation Computation:
For each time t, compute $\gamma_t(i)$ and$\xi_t(i,j)$.

3) Parameter Update:

$$\pi_i = \gamma_1(i)$$

$$a_{ij} = \frac{\sum_{t=1}^{T-1} \xi_t(i,j)}{\sum_{t=1}^{T-1} \gamma_t(i)}$$

$$\mu_i^{(k+1)} = \frac{\sum_{t=1}^{T} \gamma_t（i） o_t}{\sum_{t=1}^{T} \gamma_t(i)}$$

$$\sum_i^{（k+1）} = \frac{\sum_{t=1}^{T} \gamma_t(i)(o_t - \mu_i^{(k+1)})（o_t - \mu_i^{(k+1)}）^T}{\sum_{t=1}^{T} \gamma_t(i)}$$

4) Repeat the above steps until the model parameters converge.

Table 1: Log-likelihood value increment with number of iterations

iterations	Log-likelihood value	increment
1	–266.08481965	+nan
2	489.76302619	+755.84784583

3	637.60707764	+147.84405145
4	717.74690078	+80.13982314
5	719.30112589	+1.55422511
6	719.31225338	+0.01112749
7	719.31850337	+0.00624999
8	719.32370799	+0.00520462
9	719.32932772	+0.00561973
10	719.33714701	+0.00781929
11	719.35249718	+0.01535017
12	719.41035452	+0.05785734
13	720.31649064	+0.90613613
14	731.96751934	+11.65102870
15	737.44058357	+5.47306423
16	737.44110140	+0.00051783
17	737.44111545	+0.00001405
18	737.44111584	+0.00000039

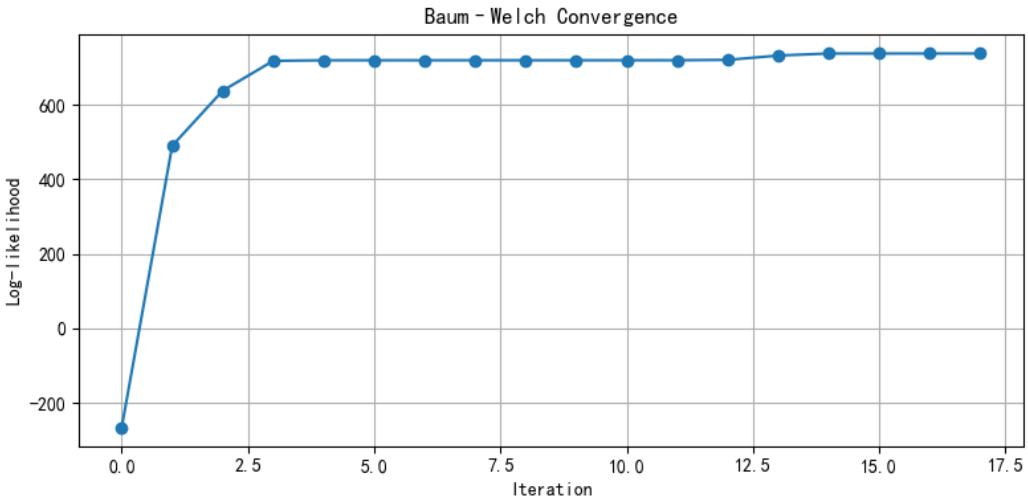

Figure 5: Convergence curve of Baum–Welch algorithm

From the convergence curve and the final parameters, the Baum–Welch algorithm's log-likelihood stabilizes at approximately 737.44 after the 18th iteration, indicating convergence. The mean vectors and covariance matrices of the Gaussian emission distributions for each state at this point are:

$$\mu_0 = \begin{pmatrix} -0.8355 \\ -0.2982 \\ 0.8033 \\ 0.8116 \\ -0.7973 \\ 0.8009 \end{pmatrix} \mu_1 = \begin{pmatrix} 0.1382 \\ 2.4166 \\ 0.1372 \\ 0.0810 \\ -0.1936 \\ 0.0398 \end{pmatrix} \mu_2 = \begin{pmatrix} 1.6580 \\ -0.1319 \\ -1.1207 \\ -1.1188 \\ 1.1068 \\ -1.1109 \end{pmatrix} \mu_3 = \begin{pmatrix} 0.8256 \\ -0.3958 \\ -1.1912 \\ -1.1842 \\ 1.2123 \\ -1.1460 \end{pmatrix}$$

$$\Sigma_0 = \text{diag}(0.001455, 0.367872, 0.235455, 0.236074, 0.226267, 0.271548)$$

$$\Sigma_1 = \text{diag}(0.579433, 0.616887, 0.327270, 0.314858, 0.299020, 0.449439)$$

$$\Sigma_2 = \text{diag}(0.009396, 0.097786, 0.006863, 0.005917, 0.016642, 0.003105)$$

$$\Sigma_3 = \text{diag}(0.161850, 0.001294, 0.000477, 0.000481, 0.007429, 0.000479)$$

5.3 Model Training

5.3.1 Sintering State Recognition

Based on the optimized parameters obtained from the Baum–Welch algorithm, an HMM is constructed. Data from Sheet2 are then read in to perform state recognition and to validate the model's accuracy.

A confusion matrix is a core tool for evaluating the performance of a classification model, as it intuitively shows the correspondence between model predictions and true labels. For the four stages of the sintering process (preheating, combustion, sintering, cooling), a 4×4 confusion matrix is constructed, with rows representing the

true classes and columns representing the predicted classes. Each element C_{ij} in the matrix denotes the number of samples whose true class is i but were predicted as class j.

$$\begin{pmatrix} 49 & 0 & 0 & 0 \\ 2 & 5 & 0 & 0 \\ 0 & 0 & 14 & 0 \\ 0 & 0 & 1 & 18 \end{pmatrix}$$

The confusion matrix shows that the model correctly identified all 49 preheating states, correctly recognized 5 of the 7 combustion states while misclassifying 2 as preheating, correctly classified all 14 sintering states, and correctly recognized 18 of the 19 cooling states with the remaining one misclassified as combustion.

Table 2: The classification performance of the model

State	Precision	Recall	F1-score	Support
preheating	0.9608	1.0000	0.9800	49
combustion	1.0000	0.7143	0.8333	7
sintering	0.9333	1.0000	0.9655	14
cooling	1.0000	0.9474	0.9730	19

The model's classification performance is presented in Table 2. Precision measures the proportion of samples predicted for a given stage that actually belong to that stage, recall measures the proportion of true samples for a stage that are correctly identified, and their harmonic mean is the F1-score. Support denotes the actual number of samples for each stage in the test set. The results indicate that the model distinguishes the preheating, sintering, and cooling stages exceptionally well—each achieving precision and recall above 0.93 and an F1-score above 0.98—while overall classification accuracy reaches 96.63%. In summary, the model demonstrates outstanding performance and can reliably support real-time identification of process stages and determination of the optimal cooling moment.

5.3.2 Sintering state prediction

Table 3: Observational data

Time	Temperature	SO_2	NO	NO_X	O_2	CO
10	51.533750	14.6	196.3	300.6	15.2	9267.5
11	52.872415	13.4	191.6	304.2	15.5	8732.0
12	52.185667	12.3	196.1	300.0	15.4	8918.8
13	52.514910	11.7	207.3	301.3	15.2	8910.3
14	52.645583	11.7	204.6	313.0	15.3	9445.0

Data from minutes 10 through 14 in Sheet 3 (Table 3) were used as the observation sequence; as shown in Figure 4.6, the model predicted entry into the cooling stage at 57 minutes, differing from the actual time by only one minute, and the overall accuracy of the state-prediction model reached 91.55%.

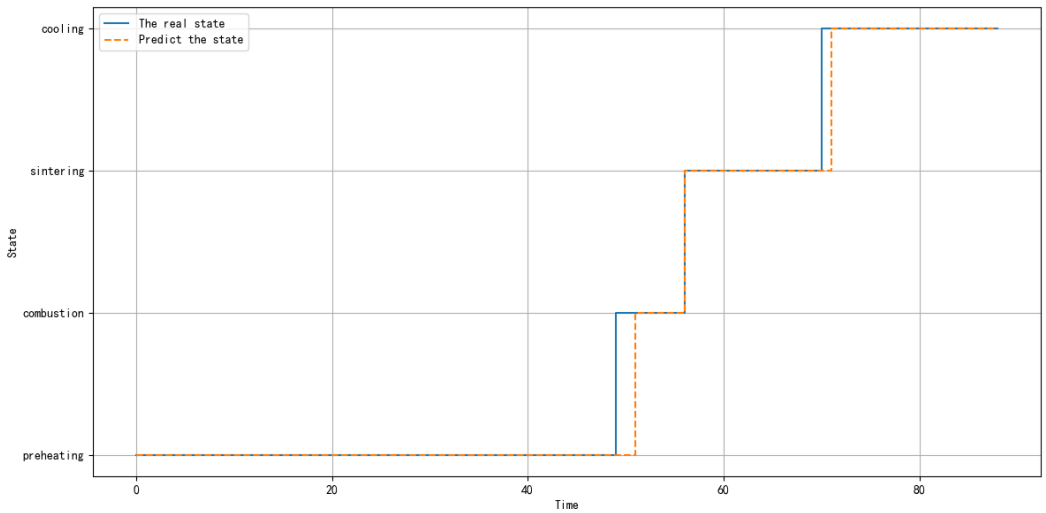

Figure 3: Comparison of the real state with the predicted state

6. CONCLUSION

This study employed a Hidden Markov Model (HMM) to model and identify the four key stages of the iron-ore sintering process—preheating, combustion, sintering, and cooling. Minute-level flue-gas monitoring data (temperature, SO_2 concentration, NO concentration, NO_x concentration, O_2 content, and CO concentration) were used to estimate the parameters of a Gaussian HMM via the Baum–Welch algorithm, and the Viterbi algorithm was applied to decode each minute's hidden state until the first detection of the "cooling" stage. Experimental results demonstrate an overall classification accuracy of 96.63%; precision and recall for the preheating, sintering, and cooling stages each exceed 93%. Although recall for the combustion stage is slightly lower (71.43%) due to limited sample size, its precision remains at 100%, providing robust support for accurately determining the cooling onset.

The primary contributions of this work include the integration of Baum–Welch parameter estimation with Gaussian emission distributions to achieve precise modeling of sintering stages, and the introduction of a "predict-until-cooling" strategy based on Viterbi decoding that offers a viable algorithmic framework for online monitoring systems. By accurately pinpointing the cooling moment, this approach helps to avoid both underburning and overburning, thereby improving raw-material utilization and reducing carbon emissions. Nonetheless, certain limitations remain: the scarcity of combustion-stage samples and feature overlap with adjacent stages resulted in occasional misclassifications, and the model exhibited sensitivity to initial parameters and convergence behavior, indicating a need for more robust initialization strategies. Future work could incorporate deep reinforcement learning to enhance model robustness and explore multi-source data fusion—such as including sinter-bed thickness or permeability as auxiliary observations, or integrating infrared thermal imaging to capture the spatiotemporal evolution of bed-temperature profiles—to further boost predictive accuracy and practical applicability.

In summary, this study validates the effectiveness of Hidden Markov Models for stage recognition and carbon-emission control in the sintering process, offering valuable technical guidance for online monitoring and intelligent emission reduction in the steel industry.

ACKNOWLEDGEMENTS

This article is supported by the Undergraduate Entrepreneurship Training Program of North China University of Science and Technology. Project numbers: T2023068, X2023137.

REFERENCES

[1] World Steel Association. World Steel in Figures 2024 [M]. Beijing: Metallurgical Industry Press, 2024.
[2] ZHU Tingyu, LI Yuran. Sintering Flue Gas Emission Control Technology and Engineering Applications [M]. Metallurgical Industry Press, 2015.
[3] WANG Xindong, HOU Changjiang, TIAN Jinglei. Multi-pollutant cooperative control technology for flue gas in the iron and steel industry and its application practice [J]. Chinese Journal of Process Engineering, 2020, 20(9): 997-1007.
[4] ZHAO Xinfeng, QI Xiwei, CHENG Yang, et al. Analysis of flue gas emission patterns during iron ore sintering process [J]. Journal of Iron and Steel Research, 2022, 34(8): 758-767.
[5] Fernández-González D, Ruiz-Bustinza I, Mochón J, et al. Iron ore sintering: Process [J]. Mineral Processing and Extractive Metallurgy Review, 2017, 38(4): 215-227.
[6] HU Jiulin, ZHOU Haoyu, LIU Qian, et al. Mechanism of CO generation in iron ore sintering process and key technologies for emission reduction [J/OL]. China Metallurgy, 1-10 [2025-03-06].
[7] Nguyen L. Tutorial on hidden Markov model [J]. Applied and Computational Mathematics, 2017, 6(4-1): 16-38.
[8] Blunsom P. Hidden markov models [J]. Lecture notes, August, 2004, 15(18-19): 48.
[9] BAUM L E, PETRIE T. Statistical inference for probabilistic functions of finite state Markov chains [J]. The Annals of Mathematical Statistics, 1966, 37(6): 1554-1563.
[10] VITERBI A J. Error bounds for convolutional codes and an asymptotically optimum decoding algorithm [J]. IEEE Transactions on Information Theory, 1967, 13(2): 260-269.